Optimal Design and Analysis of a Mixed Airfoil Blade for Small-Scale HAWTs

Geneti Temesgen Terefa
Department of Mechatronic Engineering, Pan African University Institute for Basic Sciences Technology and Innovation, Nairobi, Kenya
temesgen.geneti@students.jkuat.ac.ke (corresponding author)

Jackson Githu Njiri
Department of Mechatronic Engineering, Jomo Kenyatta University of Agriculture and Technology (JKUAT), Juja, Kenya
jackgithu@eng.jkuat.ac.ke

Patrick Irungu Muiruri
Department of Mechanical Engineering, Jomo Kenyatta University of Agriculture and Technology (JKUAT), Juja, Kenya
pmuiruri@jkuat.ac.ke

Chala Merga Abdissa
School of Electrical and Computer Engineering, Addis Ababa University, Addis Ababa, Ethiopia
chala.merga@aait.edu.et

Received: 17 January 2025 | Revised: 11 February 2025 | Accepted: 22 February 2025

 DOI: https://doi.org/10.48084/etasr.10275

ABSTRACT

This study investigates the optimum aerodynamic performance of small-scale Horizontal Axis Wind Turbines (HAWTs) utilizing a mixed-airfoil blade design. The QBlade software was employed for the selection of the best performing airfoils based on the lift-to-drag ratio and a range of operational performance. Additionally, the Blade Element Momentum (BEM) theory was deployed for the analysis of the blade's design and performance. Finally, in Computational Fluid Dynamics (CFD), the SST k-ω turbulent model was also applied for better analysis. The key findings demonstrated that the optimal airfoils including SG6040 (root), NACA 4711 (middle), and SG6043 (tip), were chosen based on their superior lift-to-drag ratio and structural integrity. Furthermore, the designed mixed-airfoil blade achieved power coefficients of 0.454 (BEM), 0.432 (QBlade), and 0.395 (CFD) at a Tip Speed Ratio (TSR) of 5.5, which are greater than the conventional single-airfoil designs. It was concluded that mixed-airfoil configurations significantly enhance the aerodynamic efficiency of small scale wind turbines, and that future research on structural analysis and torque control mechanism integration is essential to further optimize performance and energy capture.

Keywords-wind energy; small-scale HAWTs; airfoils; Blade Element Momentum (BEM) theory; CFD

I. INTRODUCTION

Wind energy is a rapidly developing power generation technology utilizing renewable resources [1, 2]. The wind energy capacity has increased in a global scale from 198 GW (2010) to 906 GW (2022), and it is expected to have reached nearly 1 TW by 2030 [3]. Figure 1 presents the overall wind energy power installed between 2010 and 2023 [4]. Wind turbines are crucial for converting the kinetic energy in the air to electric power [5]. The former are categorized into two types: HAWTs and Vertical Axis Wind Turbines (VAWTs). HAWTs exhibit better efficiency, especially in larger designs compared to VAWTs [5-7].

Large wind turbines need a lot of space to be installed, with typical rotor diameters ranging from 50 to 100 m. These turbines can produce approximately 1 to 3 MW of power, which means that they demand high construction costs and they cause noise issues that will probably annoy local communities [8]. In contrast, small HAWTs are better for both residential and remote areas, with low-wind speed. That kind of turbines has rotor diameters of 1.25 to 10 m, generating 0.25 to 16 kW, while small commercial turbines (10 to 20 m in diameter) can

produce up to 100 kW, as detailed in Table I [9]. Small Scale Wind Turbines (SSWTs) produce less energy compared to large scale ones due to aerodynamic limitations. Inefficient yaw and pitch adjustments, fluctuating wind behavior, and the lack of ability to optimize blade aerodynamics effectively are some examples of these restrictions. A key factor in wind turbine performance is the blade design, which directly affects power generation efficiency. Traditional SSWT blades typically employ single-airfoil designs, which reduce the performance and cannot be adapted to different wind conditions.

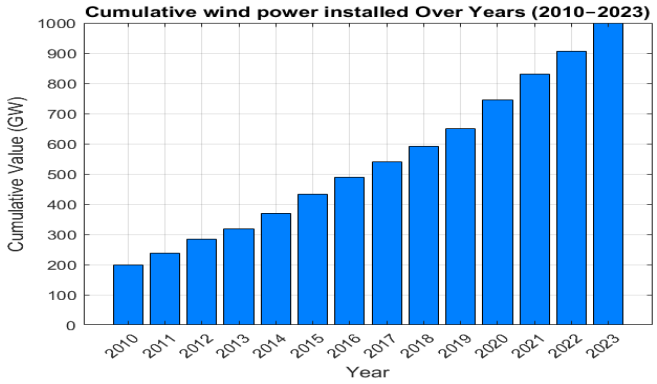

Fig. 1. Cumulative installed wind power capacity worldwide from 2010 to 2023.

TABLE I. CLASSIFICATION OF WIND TURBINES BASED ON ROTOR DIAMETER AND POWER RATING

Type		**Rotor diameter (m)**	**Power rating (kW)**
Small scale	Micro	< 1.25	< 0.25
	Mini	1.25-3	0.25-1.4
	Household	3 -10	1.4-16
Small commercial		10-20	25-100
Medium commercial		20-50	100-1000
Large commercial		50-100	1000-3000

Previous studies have examined the optimal choice of airfoil solution. Specifically, authors in [10] investigated an optimum solution for small-scale HAWTs by evaluating seven airfoils (NACA 0012, S1223) at a Reynolds number of 100,000. They chose the one with the highest glide ratio foil, and optimized blade parameters, such as chord and twist, using the BEM method. This technique resulted in improved lift, drag, and power coefficients, with the power output having been analyzed across varying air densities. In [11], airfoils, such as NACA 0012, 4412, 6409, and NACA 4412, were evaluated. At a 6° Angle Of Attack (AOA), a lift-to-drag ratio of 40.16 was observed, showing better performance compared to other airfoils. The S822 (tip) and S823 (root) airfoils, created by the National Renewable Energy Laboratory and Airfoil Inc. with 1-5 kW of power and 3-10 m rotor diameter, have a limited maximum lift coefficient, low drag, and are unaffected by surface roughness. Airfoil thickness affects performance, with thinner designs improving efficiency and thicker ones providing more structural strength [12, 13] Authors in [2] selected ten low Reynolds number airfoils, including BW-3, E387, FX 63-137, S822, S834, SD7062, SG6040, SG6043, SG6051, and USNPS4, to evaluate their performance, in a 1 kW wind turbine. The findings revealed that SG6043 exhibited the highest power coefficient, while the BW-3 included the shortest startup time. These parameters influence their performance in windy and low-wind areas, respectively. Furthermore, authors in [14] selected the NACA 4418 airfoil using the QBlade software for its high lift-to-drag ratio of 47 as the best choice among the other options. However, while previous studies examined the optimum airfoil selection, they failed to investigate low Reynolds numbers directly computed based on low wind speed. Notably, the impact of mixed airfoils on aerodynamic efficiency was not considered.

The aerodynamic efficiency of wind turbine blades is evaluated using the BEM theory, combining the blade element and momentum theories. The mass and momentum conservation laws are utilized to calculate the forces on each blade section, enabling thrust, power output, and efficiency estimations through iterative methods [15-16]. Additionally, the blade is divided into smaller elements to improve performance using various airfoils, enhancing energy capture and durability. However, it lacks in capturing real-time turbine dynamics. To address this, CFD tools are utilized for more accurate estimates [16-19]. For example, authors in [18] examined the aerodynamic characteristics of a newly designed three-bladed HAWT, combining the BEM theory and CFD method. They focused on the effects of TSR on efficiency and flow behavior at a wind speed of 8 m/s. The findings included pressure coefficients and velocity vectors at five radial positions, enhancing the understanding of wind turbine aerodynamics.

SSWTs are becoming popular for power generation, in low-wind-speed remote areas. However, their efficiency is often limited due to poor aerodynamic performance influenced by the blade design. This research introduces a mixed-airfoil configuration for SSWT blades to optimize aerodynamic efficiency across different blade sections. The most suitable airfoil for small-scale HAWTs is selected based on its lift-to-drag ratio and structural integrity using QBlade software. Additionally, BEM theory, QBlade simulations, and CFD are combined to validate the aerodynamic performance, ensuring a comprehensive assessment of the proposed design.

II. METHODOLOGY

Based on a literature review and the UIUC database, twenty low-Reynolds number airfoils for small-scale wind turbines were selected, as shown in Table II [14, 19-20]. The selection factors included Reynolds number, airfoil thickness, geometrical configuration, and camber properties. The QBlade software was then utilized to evaluate the selected airfoils' glide ratios and stall angles to identify the most suitable airfoils for different blade sections. This approach emphasized the importance of a high lift-to-drag ratio in improving aerodynamic efficiency for wind turbine rotors. A flowchart of this procedure is depicted in Figure 2.

The wind speed for this purpose ranged from 3 m/s to 7 m/s. The corresponding Reynolds numbers were determined using the relative velocity of the free stream wind and the tangential velocity of the rotor, calculated from the airfoil

velocity triangle. These Reynolds numbers were then computed using an average chord length of 0.05 m based on (1), with the results being presented in Table III. The AOA ranged from - 5 to 20 degrees for each blade section.

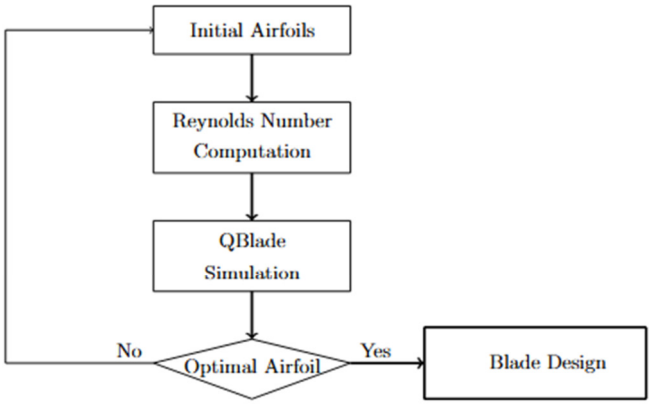

Fig. 2. Airfoil investigation flowchart.

TABLE II. AIRFOILS FOR SECTIONS OF THE BLADE

No.	Name	t/c ratio (%)	t/c at (%)	Camber (%)	Camber at (%)
1	EPPLER 407	14.43	38.30	3.50	71.60
2	WORTMANN FX 66-17A-175	17.52	33.90	4.16	40.20
3	WORTMANN FX 60-126	12.59	2.90	3.56	56.50
4	NACA 0012	12	30.00	0.00	19.90
5	NACA 4711	11	29.10	4.00	68.40
6	NACA 4412	12.02	30.00	4.00	40.00
7	S1223	12.14	19.90	8.67	49.00
8	SD706	13.98	27.22	3.97	38.82
9	S121O	12	21.51	7.20	51.11
10	SG6043	10.02	32.10	5.50	49.70
11	GOE 457	7.83	19.90	4.22	39.90
12	EPPLER 856	18.15	31.80	4.25	50.10
13	NACA 0024	24.01	30	0.00	12.50
14	NACA 2424	24	29.70	2.00	40.00
15	NACA 4418	18.02	30.0	4.00	40.00
16	NACA 4424	24.02	29.10	4.00	39.50
17	NREL's S833	18	36.30	2.52	78.70
18	NREL's S809	20.99	38.30	0.99	82.30
19	SG6050	16.01	31.53	3.24	45.33
20	SG6040	16	35.32	2.50	60.41

TABLE III. REYNOLDS NUMBERS CORRESPONDING FREE STREAM WIND VELOCITY

Free stream wind velocity, V_∞ (m/s)	*V* tangential (m/s)	*V* relative (m/s)	*Re*
3	16.5	16.77	70,258
4	22.0	22.36	93,826
5	27.5	27.95	117,393
6	33.0	33.54	140,961

The Reynolds number is given by:

$$Re = \frac{Uc}{v} \quad (1)$$

$$\lambda = \frac{\omega r}{U} \quad (2)$$

where c denotes the chord width, U is the wind speed, and v is the kinematics viscosity of the air.

The blade design procedure starts with the selection of various rotor parameters and the choice of an airfoil. The power output from a wind turbine can be calculated using:

$$P = \frac{1}{2} C_P \rho v^3 \pi R^2 \quad (3)$$

where P represents the power, C_p is the power coefficient, ρ is the air density, v is the free stream velocity, and R is the rotor radius. The required power output was set to 50 W based on Table I, with a selected wind speed of 6 m/s to achieve this power value. The power coefficient, C_p, was assumed to be 0.45. Using these values, the rotor radius was calculated from (2) to be approximately 0.5 m, with a hub radius of 0.08 m, resulting in an effective radius of 0.42 m. The next step involved choosing a TSR, λ. For electrical power generation, TSR ranged from $4 < \lambda < 7$ [21].

In this study, a TSR of 5.5 was obtained using (2). Generally, wind turbines utilize three blades, since the power increase is insignificant if more than three blades are used. The blade was then divided into N elements. Optimized Schmitz theory, stated in (3) and (4), was used to determine the chord length (c) and twist angle (β) at each element:

$$c = \frac{16\pi r}{BC_L}\left(Sin\left(\frac{1}{3}tan^{-1}\frac{1}{\lambda_r}\right)\right)^2 \quad (4)$$

$$\beta = \left(\frac{2}{3}tan^{-1}\frac{1}{\lambda_r}\right) - a \quad (5)$$

The blade's performance is evaluated, and the appropriate parameter modifications can be made based on the optimized induction factors. To achieve optimal results, both the axial and angular induction factors should be adjusted. The iterative procedure starts by assuming initial values of a and a'. Next, the angle ϕ is computed, followed by the determination of lift and drag coefficients for the desired AOA. Then, a and a' are recalculated using (6) and (7), respectively, and they are considered correct if their difference with the initial values does not exceed 2%. Otherwise, the process is repeated util this difference is reached, as detailed in Figure 3.

The BEM theory is a theoretical approach to calculate the performance of a wind turbine blade. To optimize the wind turbine results, the axial (a) and rotational (a') induction factors must be adjusted. The first step is to estimate each blade element's induction factor. The optimum induction factor can be determined iteratively by:

$$a = \frac{1}{\frac{4F(sin\,\phi)^2}{\sigma C_y} + 1} \quad (6)$$

$$a' = \frac{1}{\frac{4F(\sin\phi\cos\phi)}{\sigma C_x} - 1} \quad (7)$$

Prandtl's tip loss is considered to account for the loss near the tips of the blade using:

$$F = \frac{2}{\pi} cos'\left(\exp\left(-\frac{B}{2}\frac{R-r}{r\sin\phi}\right)\right) \quad (8)$$

where C_y is the normal force coefficient, C_x is a tangential force coefficient, ϕ is the flow angle, and σ is the solidity ratio. Then the overall power coefficient is computed by:

$$c_P = \frac{8}{\lambda^2}\int_{\lambda_0}^{\lambda} F_{\lambda r} a'^3 (1-a)\, d\lambda_r \quad (9)$$

The QBlade software tool is also utilized to analyze the blade's performance. It is a simple tool for wind turbine design [22]. Initially, the airfoils selected for each blade section are imported. The XFOIL direct airfoil method is then applied, followed by polar extrapolation to 360 tabs, which extrapolate a circle with a diameter equal to the chord of each airfoil. The initial blade shape obtained from BEM is used to model the blade in the Qblade HAWT rotor design tab. Then, simulation parameters and analysis settings are being set in the rotor BEM simulation tab.

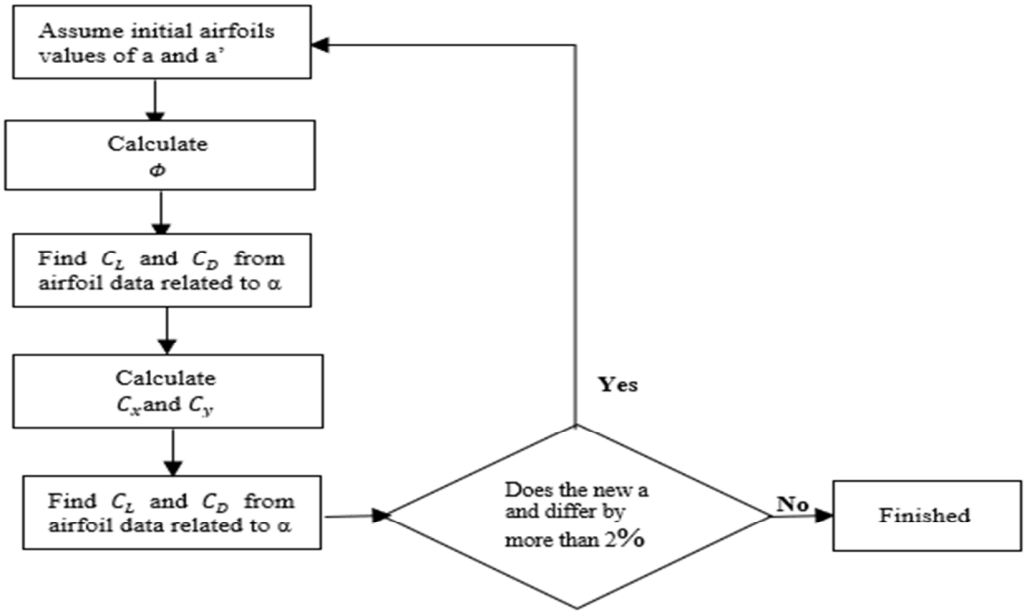

Fig. 3. Axial and rotational induction factor optimization flowchart.

The numerical analysis for this study was performed using CFD analysis in ANSYS Fluent. The blade geometry was modeled using the ANSYS Design Modeler, as depicted in Figure 4. To decrease the number of mesh cells, only one-third of the flow domain and a single blade were simulated, as displayed in Figure 5. The Frustum of Cone domain was used over other geometries, such as rectangular or cylindrical domains, due to its unique advantages in applications involving conformal arrays and fluid dynamics.

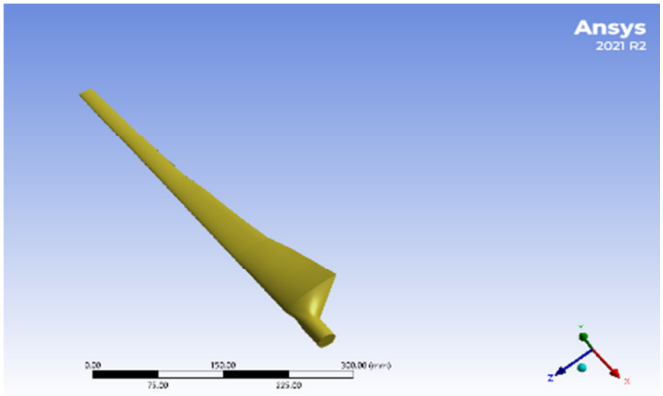

Fig. 4. CFD pre-processing: blade geometry.

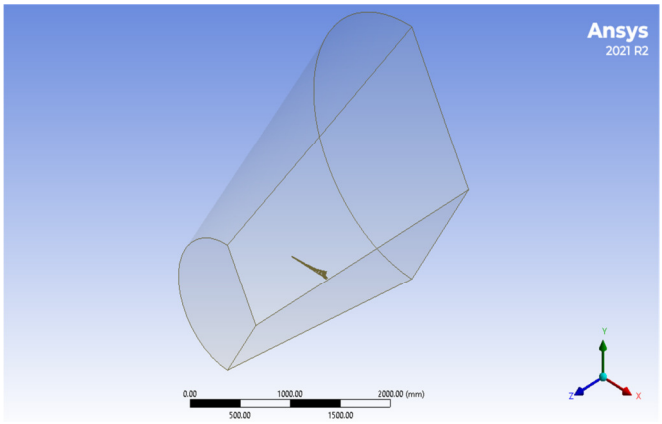

Fig. 5. CFD pre-processing: domain.

The global mesh was developed with an element size of 80 mm. Local mesh controls, blade face sizing with a mesh element size of 1 mm, twenty inflation layers with a growth rate of 1.2, and a sphere of influence with an element size of 20 mm around the blade surface were employed for better quality. The final mesh consisted of 5,226,003 elements. Figure 6 illustrates the mesh around a blade surface, Figures 7 and 8 depict the mesh quality metrics with average skewness of 0.22 and average orthogonal of 0.82, respectively.

The mesh was then transferred to the Fluent solver, where a steady-state pressure-based solver was utilized to solve continuity and momentum Navier-Stoke equations with the k-ω SST turbulent model taken as closure. Pressure and velocity were decoupled through the SIMPLE algorithm and discretization scheme specified to second order upwind for momentum, turbulent kinetic energy, and dissipation rate, while the pressure interpolation scheme was settled to second order. The SST k-ω turbulence model was selected for its advanced ability to obtain flow separation and boundary layer effects, making it more suitable for wind turbine aerodynamics compared to standard k-ε models. The inlet velocity was set at 6 m/s, aligning with the design conditions, while the outlet was maintained at atmospheric pressure. A no-slip condition was applied to the blade surface to accurately model viscous effects. To optimize computational efficiency, symmetry conditions were enforced on the top and side domains, and periodic boundary conditions were applied on opposite faces to simulate the full rotor behavior. The model achieved convergence after 3,000 iterations, with residuals dropping below 10^{-6}, ensuring numerical stability and reliability.

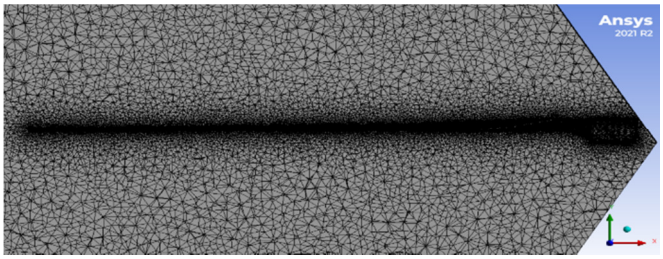

Fig. 6. Mesh around blade surface.

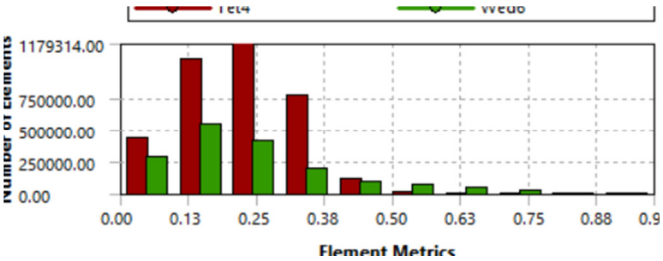

Fig. 7. Skewness mesh quality metrics.

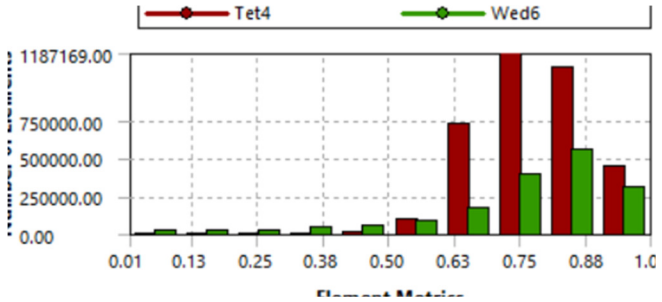

Fig. 8. Orthogonal mesh quality metrics.

III. RESULTS AND DISCUSSION

The root part of the blade is critical to its structural strength but is not significantly related to power generation. Therefore, a thickness-to-chord ratio greater than 15%, such as NACA 0024, NREL's S833, and SG6040, was considered for this part. Figures 9 and 10 illustrate the lift-to-drag ratio (C_L/C_D) against AOA for the root section at the minimum and maximum Reynolds numbers. All airfoils exhibited improved aerodynamic efficiency at high Re = 140,961, with much higher C_L/C_D values compared to Re = 70,258. The SG6040 airfoil achieved the highest C_L/C_D ratio at both Reynolds numbers. Figures 11 and 12 display the same analysis for the blade's mid-section, which plays a crucial role in preserving both structural integrity and aerodynamic efficiency. This section acts as a smooth transition between the root and tip areas of the blade. At Re = 70,258, the airfoils exhibited lower C_L/C_D values, with their performance declining sharply once they exceed their peak AOA. Among the tested airfoils, the NACA 4711 achieved the highest C_L/C_D value of approximately 55 at 6° AOA.

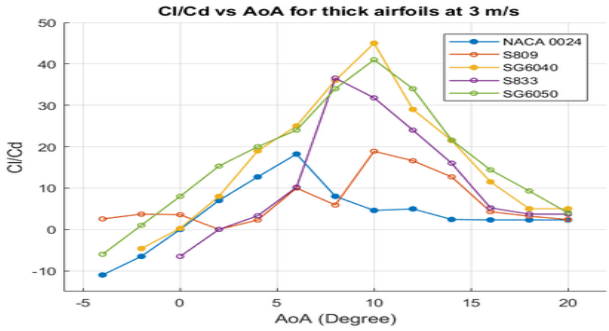

Fig. 9. Root section airfoils C_L/C_D against AOA at Re = 70,258.

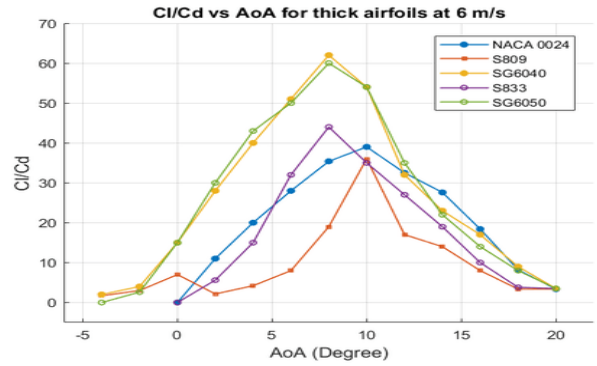

Fig. 10. Root section airfoils C_L/C_D against AOA at Re = 140,961.

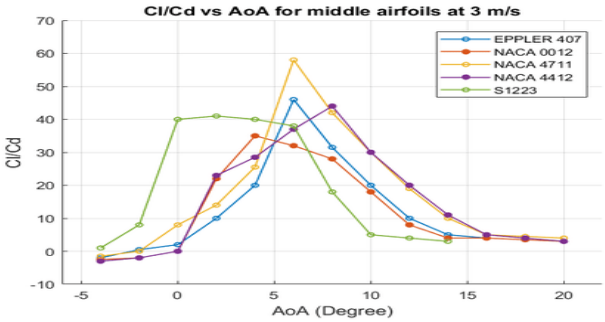

Fig. 11. Middle section airfoils C_L/C_D vs AOA at Re = 70,258.

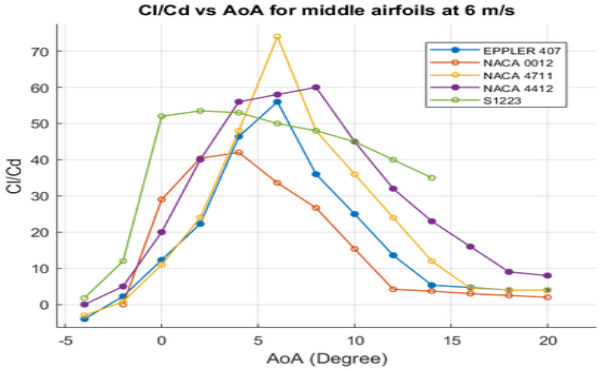

Fig. 12. Middle section airfoils C_L/C_D against AOA at Re = 140,961.

When the Reynolds number rises to 140,961, all airfoils show marked improvements in aerodynamic efficiency, with higher C_L/C_D values. The NACA 4711, Eppler 407, and NACA 4412 airfoils exhibited the highest peaks, with C_L/C_D ranging from 60 to 70, offering broader operational AOA ranges. The S1223 airfoil, which performs weakly at lower Reynolds numbers, demonstrates significant enhancement at higher Reynolds numbers, with a C_L/C_D of 60. For micro-HAWTs, NACA 4711 is ideal for low wind speeds, while the NACA 4711, Eppler 407, and NACA 4412 are optimal for higher wind speeds.

The airfoils with a thickness-to-chord ratio of less than 15 % for the tip section, which significantly contributes to aerodynamic efficiency, have also been investigated, as shown in Figures 13 and 14. At a Reynolds number of 70,258, C_L/C_D values ranged from 40 and 60. The SG6043 reached 60 at 6° AOA but dropped sharply post-stall, while the S1210 airfoil peaked at approximately 50 at 2° AOA.

At a higher Reynolds number of 140,961, all airfoils showed improved C_L/C_D performance and delayed stall. The SG6043 airfoil reached nearly 90 at 6° AOA, and the S1210 followed with 75 at 4° AOA. The GOE 457 and FX 60-126 airfoils also demonstrated better operational ranges and smoother post-stall behavior. For small-scale HAWTs, SG6043 and S1210 are great solutions due to their excellent aerodynamic efficiency and broader operational range. In summary, considering the aerodynamic performance of the airfoils represented by the lift-to-drag ratio (C_L/C_D), their broader operational range, and geometric features, the following airfoils were selected for the wind turbine blade design: SG6040 for the root section, NACA 4711 for the middle section, and SG6043 for the tip section.

Each blade element's chord length and twist angle should be determined before proceeding to the BEM theory. The blade was split into 13 segments, and for each segment the chord and twist angle are defined by (4) and (5), respectively. Figures 15 and 16 illustrate the chord length and twist angle computed for each blade element. In the BEM analysis, the number of blade design variables (parameters) was assumed to continue with the analysis. Wind speed was taken as 4.5 m/s (the average speed of the design), and the radius of the rotor was obtained as 0.5 m with the hub.

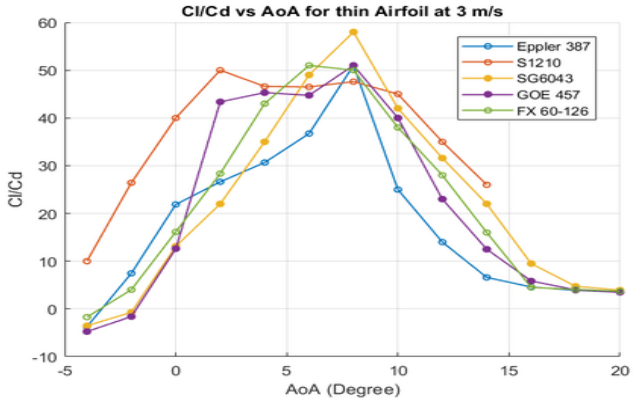

Fig. 13. Tip section airfoils C_L/C_D against AOA at Re = 70,258.

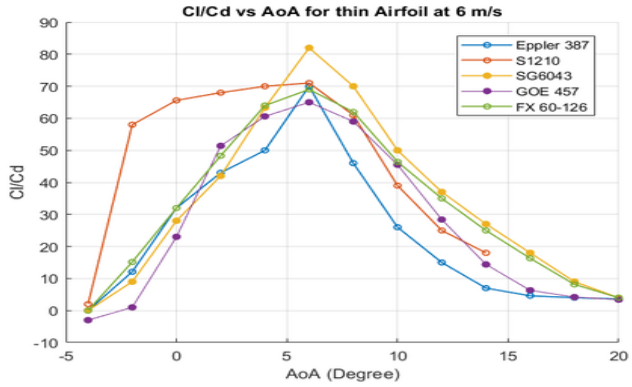

Fig. 14. Tip section airfoils C_L/C_D against AOA at Re = 140,961.

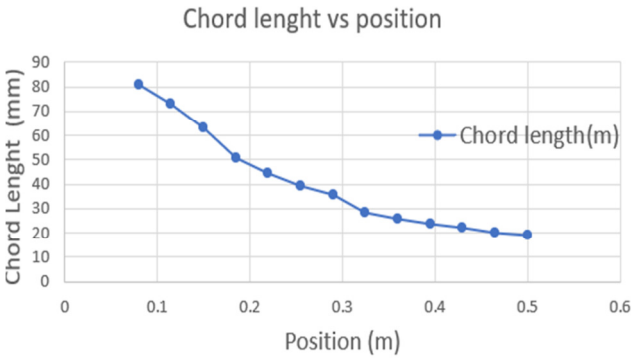

Fig. 15. Chord length distribution along the blade span.

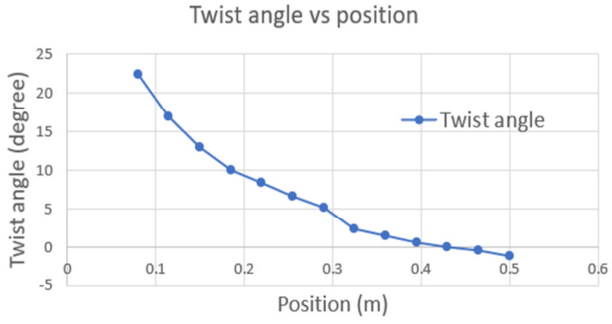

Fig. 16. Twist angle distribution along the blade span.

Table IV presents the computed flow angle, optimized axial and rotational induction flow, and Prandtl's tip for each blade segment. The power coefficient obtained is 0.454, TSR of 5.5.

TABLE IV. RESULTS OF AXIAL, ROTATIONAL INDUCTION, PRANDTL'S TIP LOSS, AND FLOW ANGLE

R (m)	F	a	a'	ϕ (deg)
0.08	1.0000	0.2046	0.2136	31.82
0.115	0.9999	0.1518	0.1110	26.56
0.15	0.9997	0.1251	0.0712	22.26
0.185	0.9993	0.1108	0.0486	19.00
0.22	0.9983	0.0951	0.0355	16.60
0.255	0.9961	0.0828	0.0269	14.73
0.29	0.9917	0.0733	0.0212	13.21
0.325	0.9825	0.0684	0.0171	11.94
0.36	0.9635	0.0629	0.0143	10.90
0.395	0.9247	0.0596	0.0125	10.00
0.43	0.8448	0.0597	0.0116	9.21
0.465	0.6724	0.0689	0.0125	8.44
0.5	0.0000	1.0000	-1.0000	6.65

Figures 17 illustrates the power coefficient results, derived from the Qblade analysis. It is evident that there is a close agreement between the results from the BEM analysis and from Qblade software. The power coefficient calculated using Qblade is 0.43, while the BEM analysis yielded a coefficient of 0.454. The deviation arises because Qblade considers factors, such as hub loss, root loss, and three-dimensional effects.

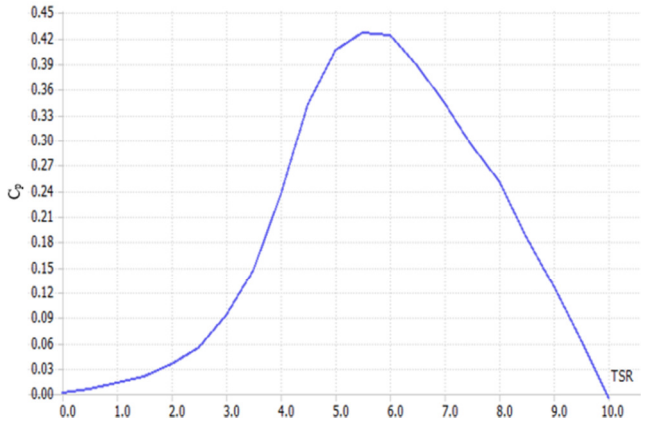

Fig. 17. Qblade performance analysis: power coefficient.

The CFD was used to visualize the simulation results, showing pressure and velocity contours around different blade spans. Figures 18-20 portray the pressure contour at 25%, 50%, and 85% spans, respectively, corresponding to the root, middle, and tip sections. At 25% span, a high-pressure region near the leading edge indicates significant stagnation, contributing mainly to structural loads rather than lift. The pressure distribution at 50% span becomes more uniform, with a wider high-pressure zone at the leading edge and a pronounced low-pressure area on the suction side, revealing maximum lift generation. At 85% span, the contours show a high-pressure region at the leading edge and a broad low-pressure area on the suction side, with a more gradual pressure gradient.

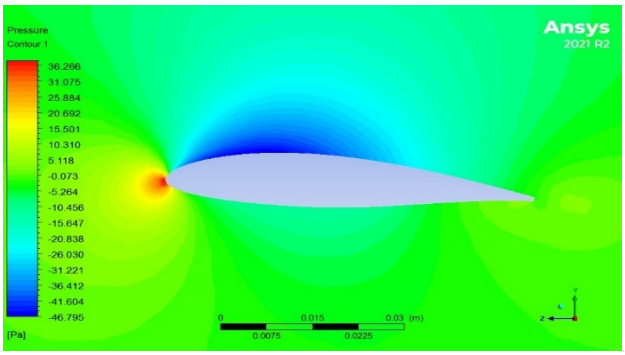

Fig. 18. Pressure contour at 25% of blade span.

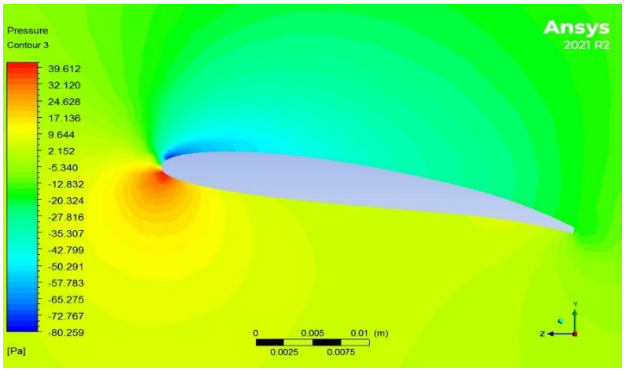

Fig. 19. Pressure contour at 50% of blade span.

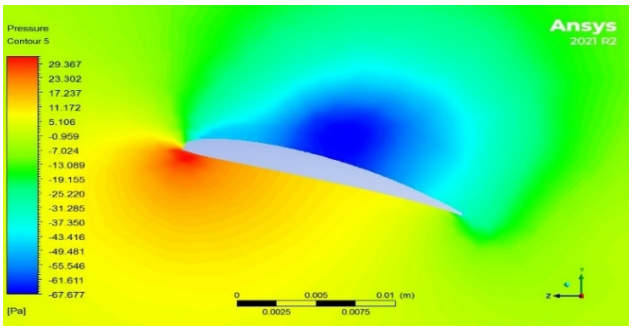

Fig. 20. Pressure contour at 85% of blade span.

The velocity contour illustrated in Figure 21 indicates distinct flow characteristics along the blade span. Near the root (25%), the flow exhibits low-energy regions with a peak velocity on the suction side and gradual flow on the pressure side, indicating lower aerodynamic loading. At mid-span (50%), Figure 22, the flow is smoother, with sharper velocity slopes, exhibiting efficient aerodynamic performance. At 85% of blade span, in Figure 23, velocities reach up to 12.2 m/s due to higher rotational speeds. Overall, velocity increases on the suction side and drops on the pressure side along the blade span, with the mid-span displaying the most efficient flow characteristics, while structural and rotational constraints influence the root and tip regions.

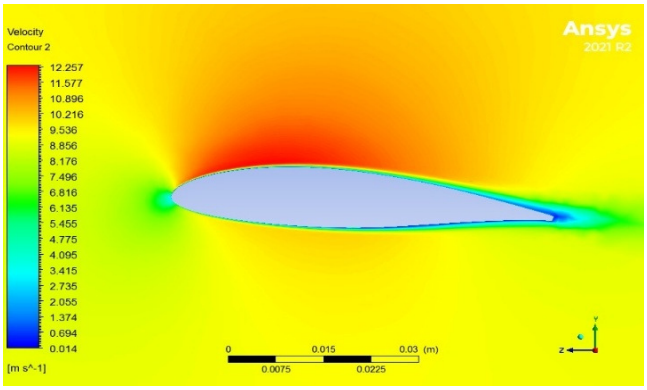

Fig. 21. Velocity contour at 25% of blade span.

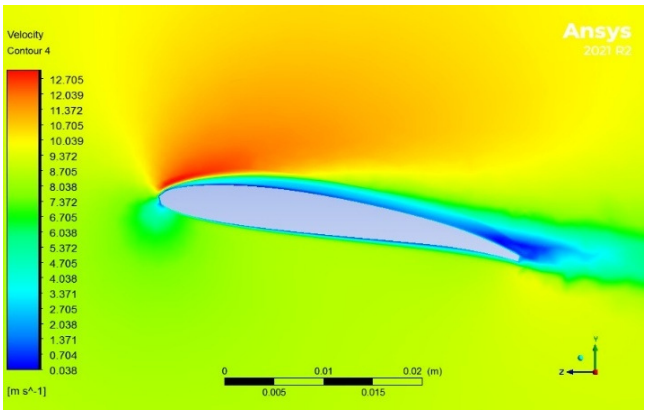

Fig. 22. Velocity contour at 50% of blade span.

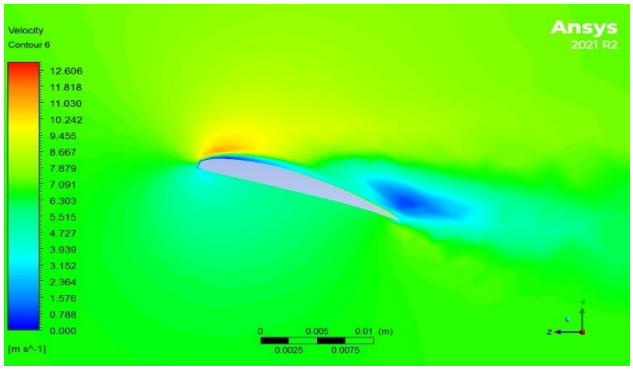

Fig. 23. Velocity contour at 85% of blade span.

Figures 24-26 depict the pressure coefficient at different blade spans. The pressure distributions suggest variations in aerodynamic behavior on different blade sections. In the root section, a high positive pressure on the pressure side near the leading edge emerges due to stagnation effects, while a low-pressure area exists on the suction side. This trend results in lower overall lift generation, as illustrated in Figure 24. In the midsection, a more balanced pressure distribution and a higher contribution to lift leads to stabilized airflow, as depicted in Figure 25. In the tip section, there is a sharp pressure gradient. The suction side displays a significant negative pressure coefficient, indicating a strong pressure drop, while the pressure side exhibits relatively moderate positive pressure, as shown in Figure 26.

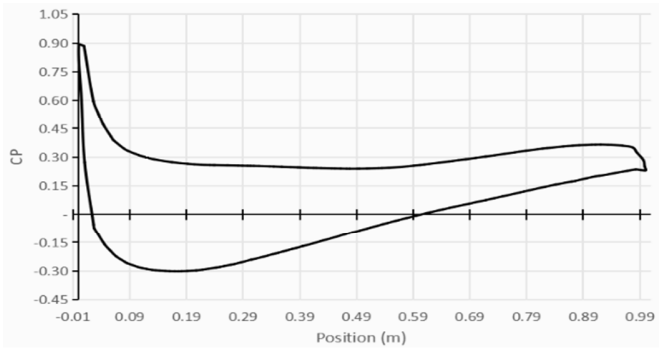

Fig. 24. Coefficient of Pressure at 25% of blade span.

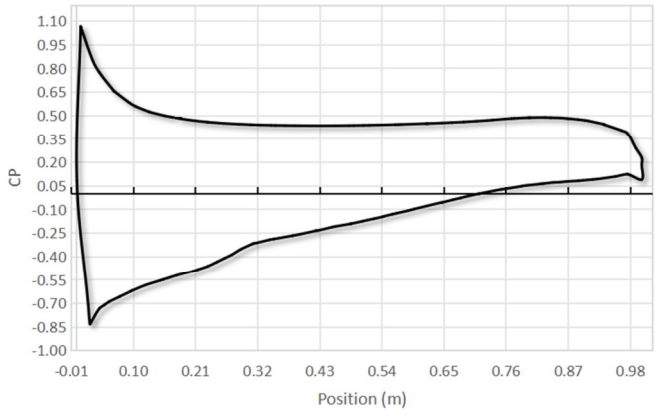

Fig. 25. Coefficient of Pressure at 85% of blade span.

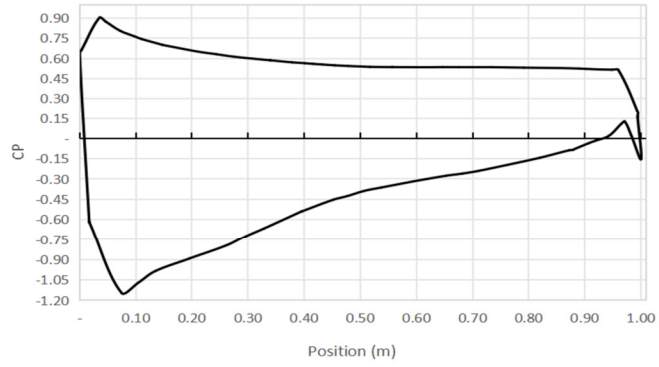

Fig. 26. Coefficient of Pressure at 85% of blade span.

Figure 27 showcases the C_p at various TSRs, comparing the results of BEM and CFD analysis. The maximum power coefficient observed was 0.454 in BEM, 0.43 in QBlade, and 0.395 in CFD. Previous work predicted the power coefficient of a mixed airfoil blade with two different airfoils as 0.343 by CFD, and 0.337 through experimental work validating the current results [1].

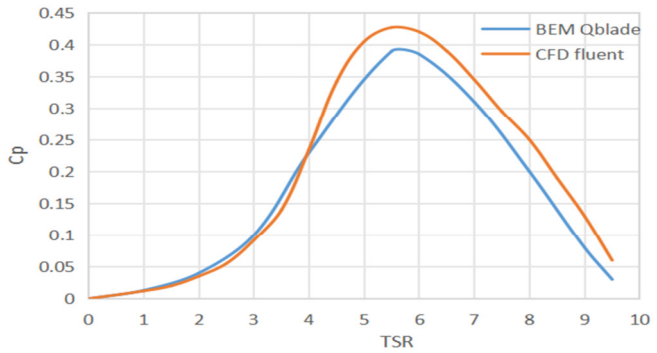

Fig. 27. Comparison of power coefficient of wind turbine in Qblade and fluent CFD analysis.

IV. CONCLUSION

This study investigated the possibility of using mixed airfoil blade designs to optimize the performance of small-scale Horizontal Axis Wind Turbines (HAWTs) in low wind conditions. It was based on selected airfoils from its aerodynamic performance that got varied Reynolds numbers. The root airfoil, SG6040, at very low lift coefficients exhibited a C_L/C_D ratio ranging from 40 to 65, ensuring structural robustness with moderate aerodynamic efficiency. At middle section, NACA 4711 achieved C_L/C_D values of 55-70, while at the tip section, SG6043 reached C_L/C_D ratios of 60-90, thereby optimizing lift while minimizing drag. The analysis utilized the Blade Element Momentum (BEM) theory, QBlade simulations, and Computational Fluid Dynamics (CFD), and the results showed power coefficients of 0.454 (BEM), 0.432 (QBlade), and 0.395 (CFD), indicating a good agreement among the methods. Further studies into the aerodynamic behavior of the designed blade were provided from the CFD results. Analyses on the contours of pressure states display that the root sections experience very high stagnation pressure, while even the middle and tip sections have well-distributed low-pressure regions efficiently contributing to lift generation. The velocity contour analysis demonstrates that the flow velocity increases from root to tip, while there is a tendency for stronger rotation speeds with higher rotational speeds at the tip to lead to stronger aerodynamic forces. All the above results verify mixed airfoil configurations, minimize aerodynamic losses, and enhance turbine efficiency across wind conditions.

Future research activities will include fluid structure interaction modeling efficiency, introduction of advanced materials with great endurance usage, cost analyses, and experimental validation in different wind conditions. Additionally, structural analysis, advanced materials to improve durability, torque control to optimize power maximization, and safe operation of turbines are critical parameters that should be investigated.

ACKNOWLEDGMENT

The authors express their gratitude to the Pan African University Institute for Basic Sciences, Technology, and Innovation (PAUSTI) for their valuable support in facilitating this study.

CONFLICT OF INTEREST

The authors declare that there are no conflicts of interest regarding the publication of this paper.

REFERENCES

[1] O. Ighodaro and D. Akhihiero, "Modeling and Performance Analysis of a Small Horizontal Axis Wind Turbine," *Journal of Energy Resources Technology*, vol. 143, no. 3, Aug. 2020, Art. no. 031301, https://doi.org/10.1115/1.4047972.

[2] V. Akbari, M. Naghashzadegan, R. Kouhikamali, F. Afsharpanah, and W. Yaïci, "Multi-Objective Optimization and Optimal Airfoil Blade Selection for a Small Horizontal-Axis Wind Turbine (HAWT) for Application in Regions with Various Wind Potential," *Machines*, vol. 10, no. 8, Aug. 2022, Art. no. 687, https://doi.org/10.3390/machines10080687.

[3] S. N. Bhadra, D. Kastha, and S. Banerjee, *Wind Electrical Systems*. Oxford University Press, 2013.

[4] J. Dorrell and K. Lee, "The Cost of Wind: Negative Economic Effects of Global Wind Energy Development," *Energies*, vol. 13, no. 14, Jan. 2020, Art. no. 3667, https://doi.org/10.3390/en13143667.

[5] Y. Kassem, H. Camur, and T. Apreala, "Assessment of Wind Energy Potential for achieving Sustainable Development Goal 7 in the Rural Region of Jeje, Nigeria," *Engineering, Technology & Applied Science Research*, vol. 14, no. 4, pp. 14977–14987, Aug. 2024, https://doi.org/10.48084/etasr.7311.

[6] T. Batu *et al.*, "Optimal airfoil selection for small horizontal axis wind turbine blades: A multi-criteria approach," *Advances in Mechanical and Materials Engineering*, vol. 41, pp. 57–68, 2024, https://doi.org/10.7862/rm.2024.6.

[7] M. A. Al-Rawajfeh and M. R. Gomaa, "Comparison between horizontal and vertical axis wind turbine," *International Journal of Applied Power Engineering (IJAPE)*, vol. 12, no. 1, Mar. 2023, Art. no. 13, https://doi.org/10.11591/ijape.v12.i1.pp13-23.

[8] M. Junginger, E. Hittinger, E. Williams, and R. Wiser, "Onshore wind energy," in *Technological Learning in the Transition to a Low-Carbon Energy System*, Amsterdam, Netherlands: Elsevier, 2020, pp. 87–102.

[9] A. Tummala, R. K. Velamati, D. K. Sinha, V. Indraja, and V. H. Krishna, "A review on small scale wind turbines," *Renewable and Sustainable Energy Reviews*, vol. 56, pp. 1351–1371, Apr. 2016, https://doi.org/10.1016/j.rser.2015.12.027.

[10] V. K. Venkateswaran, U. Fernandez-Gamiz, K. Portal-Porras, and J. M. Blanco, "Numerical study on aerodynamics of small scale horizontal axis wind turbine with Weibull analysis," *Scientific Reports*, vol. 14, no. 1, Nov. 2024, Art. no 26790, https://doi.org/10.1038/s41598-024-78503-2.

[11] Siti Amni Husna Roslan, Zainudin A. Rasid, and Ahmad Kamal Arifin Mohd Ehsan, "The Aerodynamic Performance of the Small-Scale Wind Turbine Blade with NACA0012 Airfoil," *CFD Letters*, vol. 14, no. 10, pp. 87–98, Oct. 2022, https://doi.org/10.37934/cfdl.14.10.8798.

[12] E. Y. Osei, R. Opoku, A. K. Sunnu, and M. S. Adaramola, "Development of High Performance Airfoils for Application in Small Wind Turbine Power Generation," *Journal of Energy*, vol. 2020, no. 1, Feb. 2020, Art. no. 9710189, https://doi.org/10.1155/2020/9710189.

[13] L. W. Traub and C. Coffman, "Efficient Low-Reynolds-Number Airfoils," *Journal of Aircraft*, vol. 56, no. 5, pp. 1987–2003, Sep. 2019, https://doi.org/10.2514/1.C035515.

[14] K. Muchiri, J. N. Kamau, D. W. Wekesa, C. O. Saoke, J. N. Mutuku, and J. K. Gathua, "Design and Optimization of a Wind Turbine for Rural Household Electrification in Machakos, Kenya," *Journal of Renewable Energy*, vol. 2022, no. 1, 2022, Art. no. 8297972, https://doi.org/10.1155/2022/8297972.

[15] J. Fadil, Soedibyo, and M. Ashari, "Performance comparison of vertical axis and horizontal axis wind turbines to get optimum power output," in *2017 15th International Conference on Quality in Research (QiR) : International Symposium on Electrical and Computer Engineering*, Jul. 2017, pp. 429–433, https://doi.org/10.1109/QIR.2017.8168524.

[16] A. Mezzacapo, M. C. Vitulano, A. D. Tomasso, and G. De Stefano, "CFD Prediction of Wind Turbine Blade Compressible Aerodynamics," in *23rd International Conference: Computational Science and Its Applications – ICCSA 2023*, Athens, Greece, 2023, pp. 113–125, https://doi.org/10.1007/978-3-031-36805-9_8.

[17] P. I. Muiruri and O. S. Motsamai, "Three Dimensional CFD Simulations of A Wind Turbine Blade Section; Validation," *Journal of Engineering Science and Technology Review*, vol. 11, no. 1, pp. 138–145, Feb. 2018, https://doi.org/10.25103/jestr.111.16.

[18] S. Younoussi and A. Ettaouil, "Numerical Study of a Small Horizontal-Axis Wind Turbine Aerodynamics Operating at Low Wind Speed," *Fluids*, vol. 8, no. 7, Jul. 2023, Art. no. 192, https://doi.org/10.3390/fluids8070192.

[19] E. Mollica and A. Timmoneri, "CFD analysis of the low Reynolds S1223 airfoil," *International Journal of Engineering, Science and Technology*, vol. 13, no. 4, pp. 46–49, 2021, https://doi.org/10.4314/ijest.v13i4.5.

[20] W. Yossri, S. Ben Ayed, and A. Abdelkefi, "Airfoil type and blade size effects on the aerodynamic performance of small-scale wind turbines: Computational fluid dynamics investigation," *Energy*, vol. 229, Aug. 2021, Art. no. 120739, https://doi.org/10.1016/j.energy.2021.120739.

[21] V. K. Satankar and V. Warudkar, "Modeling and aerodynamic analysis of small scale, mixed airfoil HAWT blade: A Review," *International Research Journal of Engineering and Technology*, vol. 3, no. 11, pp. 547–550, 2016.

[22] C. Sucharitha and P. Eswaraiah, "An Efficient Modeling of Wind Turbine Using QBlade Software," *International Journal of Mechanical Engineering*, vol. 7, no. 10, pp. 110–118, Oct. 2022.